5p-4f level crossing in palladium-like ions and its effect on metastable states

Naoki Kimura [1,*] Ryunosuke Kodama,[2] Priti,[2] Naoki Numadate,[2,†] Kento Suzuki,[2]
Masashi Monobe,[2] and Nobuyuki Nakamura[2]

[1]*Atomic, Molecular and Optical Physics Laboratory, RIKEN, Saitama 351-0198, Japan*
[2]*Institute for Laser Science, The University of Electro-Communications, Tokyo 182-8585, Japan*

We study the level structures of palladium-like I^{7+} ($Z = 53$) and Ba^{10+} ($Z = 56$) and the behavior of their metastable states with an electron beam ion trap. The difference in the level structures between I^{7+} and Ba^{10+} arising from the configuration crossing between $4d^{-1}5p$ and $4d^{-1}4f$ around the atomic number $Z = 56$ causes significant differences in the lifetimes of the metastable states. Ba^{10+} has several long-lived levels ($>10^{-3}$ s) in the electron configurations $4d^{-1}5s$ and $4d^{-1}4f$, whereas the lifetime of the same $4d^{-1}4f$ levels in I^{7+} is much shorter due to the appearance of deexcitation channels to a lower energy level in $4d^{-1}5p$. The extreme ultraviolet spectra identified through comparison with theoretical simulations based on a collisional-radiative model evince the level crossing between the $4d^{-1}5p$ and $4d^{-1}4f$ configurations in Ba^{10+}. Additionally, we investigate the ionization processes from the metastable states in palladium-like ions by observing the electron energy dependence of the prominent visible line ($4d^{-1} : {}^2D_{5/2}\text{-}{}^2D_{3/2}$) of rhodium-like I^{8+} and Ba^{11+}. The electron energy dependencies reflecting the properties of the metastable states show a difference between iodine and barium, which can be explained by the populations of the metastable states calculated with theoretical simulations.

I. INTRODUCTION

The palladium-like isoelectronic sequence, which has a closed $4d^{10}$ shell in the ground state, is an attractive research target for several reasons. One of them is that the relatively high excitation and ionization energies of palladium-like ions allow for their large abundance in high temperature plasmas, and induce prominent emission lines arising from their simple level structure. Thus, for astrophysical and fusion plasma diagnostics using emission spectra [1–4], the spectroscopic data of palladium-like ions are important.

Another reason involves configuration crossings in excited states. Since there are configuration crossings between $4d^{-1}5l$ ($l = s, p, d$) and $4d^{-1}4f$ for moderate atomic numbers Z ($52 \leqslant Z \leqslant 60$) as shown in Fig. 1, the energy structures of these ions show stark differences depending on the atomic number. The study of such crossings is important for the development of a new type of atomic clock using a highly charged ion (HCI) [6]. Over the last decade, many candidates for the HCI clock transition between quasidegenerate $4f$ and $5l$ levels near the crossing have been theoretically proposed [6–18], and several $5s$-$4f$ and $5p$-$4f$ level crossings have been investigated [7,19–22] by electron beam ion traps (EBITs) [23]. The systematic investigation of the palladium-like isoelectronic sequence having the $5l$-$4f$ level crossing can thus provide important knowledge for exploring these visible forbidden transitions.

The existence of metastable states is also an attractive motivation for studying palladium-like ions, since the ground state is $4d^{10}$ ${}^1S_0$, and low-lying excited levels with high angular momentum in palladium-like ions can be strongly metastable. This unique level structure with metastable states has the potential to lead to new applications. For instance, extreme ultraviolet lasing at 41.8 nm using palladium-like Xe^{8+} in a plasma was demonstrated utilizing its unique level structure [24]. Soft x-ray lasing using palladium-like W^{28+} has also been proposed [25]. Recently, another method to detect the energy of the electronic excited state by precision mass measurements has also been demonstrated by using a long-lived metastable level of palladium-like Re^{29+} [26]. Palladium-like ions are of benefit for these experiments, where strong metastable states and a large population in a plasma are needed.

The importance of metastable states in a plasma has recently been studied for EBIT plasmas and their characterizations using a collisional-radiative (CR) model calculation. For example, it has been reported that the predicted prominent emission line from the $5s$-$5p$ transition in promethium-like heavy ions does not exist in a wide range of plasma conditions due to the concentration of the population in a metastable state [20,27–29]. Ionization processes via metastable states were also studied by observing emission spectra of several HCIs at electron energies well below the threshold for ionization from the ground state of the ion of next lowest charge [30–34]. In electron-ion crossed-beam experiments, several electron configurations having highly populated metastable

---

*naoki.kimura@riken.jp
†Present address: Komaba Institute for Science, The University of Tokyo, Tokyo 153-8902, Japan.
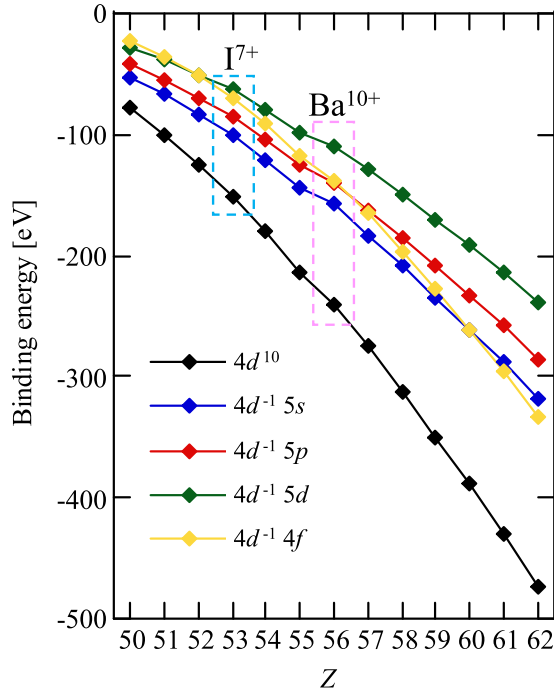
FIG. 1. Atomic number (Z) dependence of the configuration-averaged binding energies for each electron configuration of the palladium-like isoelectronic sequence calculated by the Flexible Atomic Code [5].

states which affect such ionization process have been assigned [35–38]. Such population kinetics of heavy ions with many electrons should have an atomic number dependence because the lifetime of long-lived levels involving a $4f$ electron in heavy HCIs is strongly relevant to $5l$-$4f$ level crossings. In the theoretical investigation of the level structures of Ag-, Cd-, In-, and Sn-like ions to explore visible forbidden transitions for HCI clocks, it was indicated that the lifetimes of several levels show an obvious dependence on the atomic number [12,13]. In a recent experiment, the $4f_{7/2,5/2}$-$5s$ electric octupole decays, which have long lifetimes, were directly observed for Ag-like W^{27+} in an EBIT plasma, and it was further revealed by theoretical simulations based on CR modeling that the emission intensity has a remarkable atomic number dependence due to the specific level structure including the $5d$-$4f$ level crossing [39]. For the population kinetics of palladium-like ions which have $5l$-$4f$ level crossings in the excited states, it is expected to be important to take the behavior of the metastable states into account.

Here we experimentally study level structures of palladium-like ions around the $5p$-$4f$ level crossing with an electron beam ion trap. By observing extreme ultraviolet emission spectra, we confirm the $4d^{-1}5p$ and $4d^{-1}4f$ level crossing of the palladium-like isoelectronic sequence at $Z = 56$ (Ba^{10+}) [40–43]. The electron beam energy dependence of the line intensity of rhodium-like I^{8+} and Ba^{11+} is also studied to investigate the ionization mechanism via the metastable states of palladium-like I^{7+} and Ba^{10+}. The present comparative study between I^{7+} and Ba^{10+} clearly reveals the picture of the level crossing and its contribution to the metastabilities of the long-lived levels.

II. EXPERIMENT

In the present study, highly charged iodine and barium ions were generated with a compact electron beam ion trap (CoBIT) at The University of Electro-Communications in Tokyo. The detailed description of the instrument is given in a previous paper [44]. Briefly, CoBIT consists essentially of an electron gun, a drift tube (DT), and an electron collector in an ultrahigh vacuum chamber. The drift tube is composed of three successive cylindrical electrodes (DT1, DT2, and DT3) to form an axial electrical trap potential. The electron beam emitted from the electron gun is accelerated towards the drift tube while being compressed by an axial magnetic field (typically 0.08 T) produced by a high-temperature superconductive magnet surrounding the drift tube. The compressed high-density electron beam forms the trap potential in the radial direction and successively ionizes the ions trapped in the drift tube. Iodine was introduced into the trap region through a gas injector as a vapor of CH_3I, whereas barium was introduced as a vapor from an effusion cell [45] operated at 380 °C.

The beam current I_e monitored at the electron collector with an analog meter was 2–3 mA. The electron beam energy in CoBIT is essentially determined by the voltage difference between the cathode and DT2, but it has a systematic shift and a width. The systematic shift is caused by the leakage of the electric field from DT1 and DT3 and the negative space charge potential due to the electron beam. The former potential shift is estimated to be about $+20$ V from the mechanical geometry of the DT, where $+50$ V was applied to DT1 and DT3 with respect to DT2. The space charge shift, estimated from a general space charge potential formula [31,46], is -30 to -20 V. Thus, the total systematic shift is estimated to be smaller than -10 eV. The energy width of the electron beam was previously estimated to be 5 eV with an electron beam current of 12 mA [47,48]. Although the energy width at the present experimental condition was not measured, it is expected to be less than 5 eV because the present electron beam current was much lower than that in the previous study.

Emission spectra of trapped highly charged ions in the extreme ultraviolet (EUV) region were observed with a grazing-incidence flat-field spectrometer [49] with a Peltier-cooled, back-illuminated charge coupled device (CCD) camera (Roper PIXIS-XO: 400B). The wavelength dispersion was performed with an aberration-corrected concave grating with a groove number of 1200 gr/mm (Hitachi 001-0660). The spectral resolution of the EUV measurements was typically 0.03 nm, which was mainly limited by the width of the electron beam regarded as an entrance slit. The wavelength scale was calibrated by using well-known transitions in Fe^{7+}–Fe^{14+}, Ar^{6+}–Ar^{13+}, or Kr^{8+} measured beforehand by injecting $Fe(C_5H_5)_2$ vapor, Ar or Kr gas, respectively, into CoBIT. The wavelengths of the reference lines were taken from the NIST (National Institute of Standards and Technology) database [50].

Spectra in the visible region were measured with a commercial Czerny-Turner spectrometer (Jobin Yvon HR320) with another Peltier-cooled, back-illuminated CCD camera (Andor iDus 416). For survey observations we used a 300 gr/mm grating blazed at 500 nm, whereas for wavelength

determination a high-resolution 1200 gr/mm grating blazed at 400 nm was used. The wavelength scale was calibrated with reference spectra of discharge lamps illuminated from outside of the CoBIT chamber. Prior to measurements, the stray light background mainly arising from the electron gun cathode was measured under the condition of no electron beam.

III. THEORETICAL CALCULATION

In order to analyze the EUV spectra of I^{7+} and Ba^{10+}, CR model calculations were performed using the Flexible Atomic Code (FAC 1.1.5) [5]. The present CR model includes 665 excited levels originating from $4p^64d^94f$, $4p^64d^9nl$ ($n = 5$ and 6, $l = s, p, d, f$), $4p^54d^{10}4f$, $4p^54d^{10}5l$ ($l = s, p, d, f$), and $4p^64d^85s^2$, $4p^64d^85p^2$, $4p^64d^85d^2$ and $4p^64d^85s5p$ configurations in addition to the ground state $4d^{10}$ and the first ionic state $4d^9$. Basically, intensity of an emission line can be expressed as a product of an upper level population and its transition probability for an optically thin plasma. The populations of the excited levels are obtained by solving the rate balance equations for all the excited states simultaneously as in the studied state, assuming that these levels are interconnected only through various collisional and radiative processes. In the present model, population or depopulation by electron impact excitation (de-excitation), ionization, and radiative decay were the primary considerations. Other recombination processes such as three-body recombination were ignored due to the low electron density of the EBIT plasma. Dielectronic recombination processes were not considered because they occur only when the electron beam energy is equal to the exact energy required for the dielectronic capture condition. Therefore, the rate balance equation for an excited state j, with the normalization condition $\sum_j n_j = 1$, is given by

$$\sum_{\substack{i \\ i \neq j}} k_{ij} n_i n_e + \sum_{i > j} A_{ij} n_i - \sum_{\substack{i \\ i \neq j}} k_{ji} n_j n_e$$
$$- \sum_{i < j} A_{ji} n_j - n_j n_e k_{j+} = 0.$$

Here, k_{ij}, A_{ij}, n_j, and n_e are the rate for electron impact excitation (deexcitation), the transition probability from level $i \rightarrow j$, the population of the jth level, and the electron density, respectively. Since the EBIT plasma has a quasi-monoenergetic electron distribution, the rates were calculated with a narrow Gaussian electron energy distribution function. In the present model, transition probabilities [electric-dipole allowed ($E1$) transitions within all levels, forbidden magnetic dipole ($M1$) as well as electric- and magnetic-quadrupole and octupole transitions ($E2$, $E3$, $M2$, $M3$) for levels from valance electron single excitation] and the electron excitation cross-sections among all the considered levels were taken into account. All of the required atomic data for the level energies, the transition probabilities, and the distorted-wave cross-sections were calculated from FAC 1.1.5 using wave functions obtained within the relativistic configuration interaction (RCI) approach. In the structure calculations, we have included only the above-mentioned set of configurations as this reproduced the observed spectra the best. Inclusion of more configuration

such as double excitation to $4f$ and $5f$ states and single-double excitations from the $4s$ or $3d$ inner core shifted the energy levels to higher energies. This is because, in FAC, basis wave functions are derived from a local central potential, which is self-consistently determined to represent electronic screening of the nuclear potential; inclusion of these states increases this screening. The full frequency-dependent Breit interaction in the zero-energy limit for the exchanged photon and higher-order QED effects such as self-energy and vacuum polarization corrections (treated in the screened hydrogenic approximation) were added in a subsequent (RCI) calculation [5].
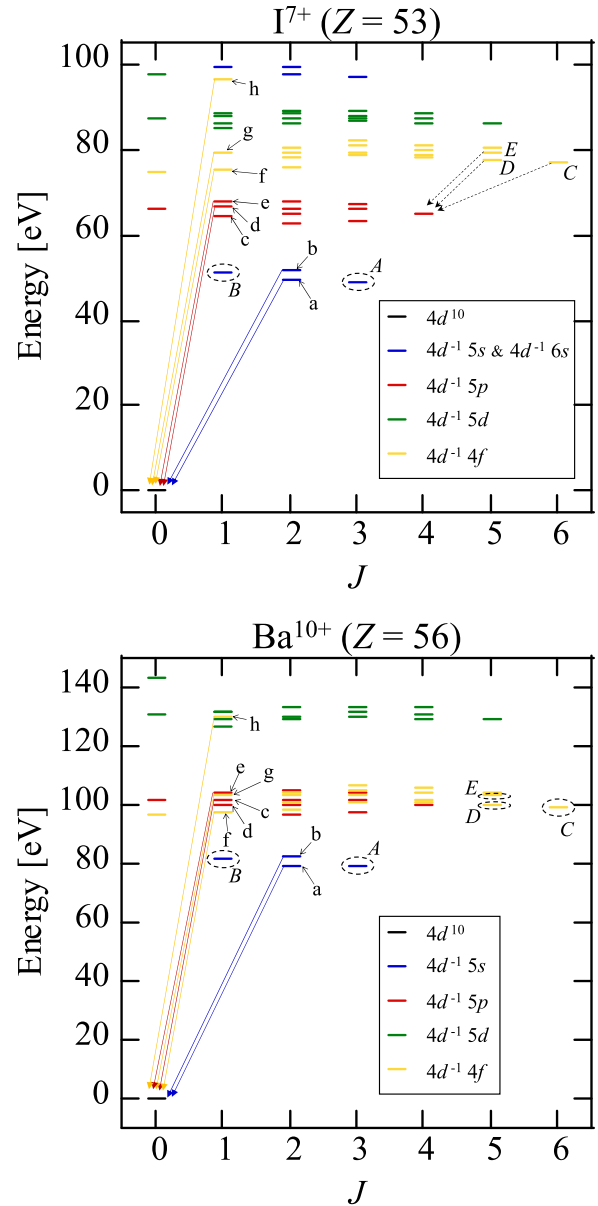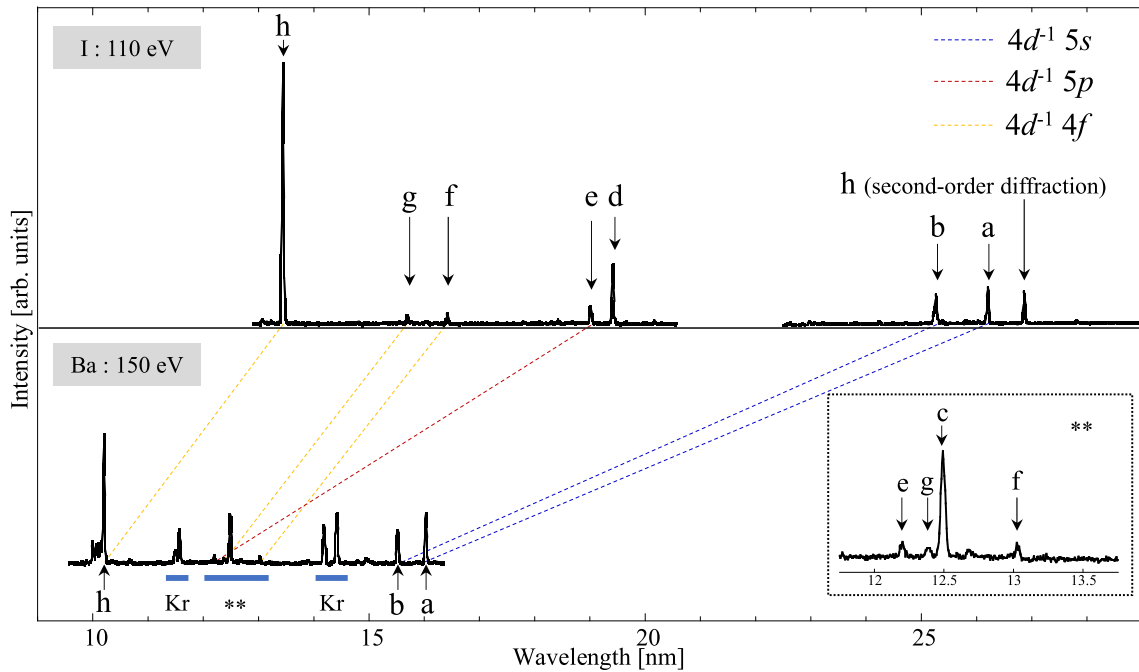

FIG. 2. Energy levels of palladium-like I^{7+} and Ba^{10+} calculated with FAC. The vertical axis shows the energy from the ground state $4d^{10}$. The horizontal axis is the total angular momentum. The energy levels are classified by their electron configurations with the color coding annotated in the graphs.
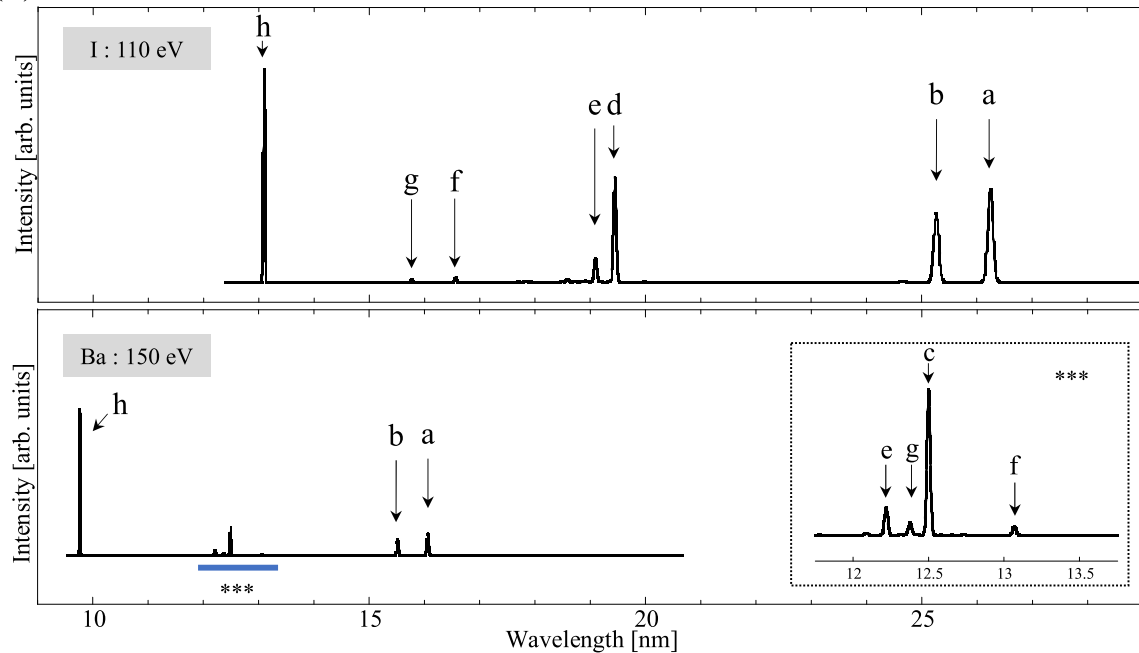
FIG. 3. Extreme ultraviolet spectra obtained by (a) experiments and (b) CR model simulations for I^{7+} and Ba^{10+}. Insets show the magnified spectra for the regions annotated with ** and ***.

IV. RESULTS AND DISCUSSION

Figure 2 shows the energy levels of palladium-like I^{7+} and Ba^{10+} calculated with FAC. The horizontal axis shows the total angular momentum. Each level is classified by color in accordance with the electron configuration. Theoretically predicted prominent transitions in our experimental condition are indicated by the solid-line arrows with the upper levels labeled a–h in Fig. 2. The metastable states whose lifetime is

longer than 1 ms are shown by the dashed-line circles labeled *A–E*. The dashed arrows indicate the *E*1-forbidden transitions with relatively large transition probability (>10^3 s^{-1}) from the levels corresponding to *C–E* in I^{7+}. In Ba^{10+}, the energy levels of the 4d^{-1}5p and 4d^{-1}4f configurations are very close to each other. In contrast, they are definitely separated in I^{7+}.

Figure 3 shows the experimentally observed spectra along with the simulated CR model spectra in the extreme ultraviolet region for I^{7+} and Ba^{10+}. The experimental spectra

TABLE I. Summary of the present and previous wavelengths (nm) for transitions in palladium-like I^{7+} and Ba^{10+}. The present theoretical and experimental wavelengths are listed as λ_{th} and λ_{ex}, respectively. The previous wavelengths λ_{ref1}, λ_{ref2}, λ_{ref3}, λ_{ref4}, λ_{ref5}, and λ_{ref6} are taken from [41–43,52–54], respectively. The present wavelengths annotated by ∗ are determined by the second-order diffraction lines. The previous wavelengths annotated by † are estimated from the energy of the upper level. The uncertainty of the present measurement is estimated to be 0.02 nm including systematic error.

| | | | $I^{7+}(Z=53)$ | | | | | |
| | | | Present | | Previous Expt. | | | Previous Theor. |
Label	Upper level	Transition type	λ_{ex}	λ_{th}	λ_{ref1}	λ_{ref2}	λ_{ref3}	λ_{ref5}
a	$\left(4d_{5/2}^{-1}\,5s_{1/2}\right)_{J=2}$	$E2$	26.21	26.24			26.2049†	
b	$\left(4d_{3/2}^{-1}\,5s_{1/2}\right)_{J=2}$	$E2$	25.27	25.27			25.2532†	
c	$\left(4d_{5/2}^{-1}\,5p_{3/2}\right)_{J=1}$	$E1$		19.98	19.6547	19.7964	19.7947	19.7852
d	$\left(4d_{3/2}^{-1}\,5p_{1/2}\right)_{J=1}$	$E1$	19.42	19.45	19.4194	19.4146	19.4155	19.4863
e	$\left(4d_{3/2}^{-1}\,5p_{3/2}\right)_{J=1}$	$E1$	19.02	19.09	19.0156	19.0157	19.0152	19.0457
f	$\left(4d_{5/2}^{-1}\,4f_{5/2}\right)_{J=1}$	$E1$	16.44	16.56	16.4181			16.5954
g	$\left(4d_{3/2}^{-1}\,4f_{5/2}\right)_{J=1}$	$E1$	15.71	15.77	15.7074	15.6976		15.7636
h	$\left(4d_{5/2}^{-1}\,4f_{7/2}\right)_{J=1}$	$E1$	13.43*	13.09	13.4327	13.4301		13.0097
			$Ba^{10+}(Z=56)$					
			Present		Previous Expt.	Previous Theor.		
Label	Upper level	Transition type	λ_{ex}	λ_{th}	λ_{ref4}	λ_{ref5}	λ_{ref6}	
a	$\left(4d_{5/2}^{-1}\,5s_{1/2}\right)_{J=2}$	$E2$	16.09	16.09	16.0845†			
b	$\left(4d_{3/2}^{-1}\,5s_{1/2}\right)_{J=2}$	$E2$	15.55	15.52	15.5454†			
c	$\left(4d_{5/2}^{-1}\,5p_{3/2}\right)_{J=1}$	$E1$	12.49	12.50	12.5042	12.5162	12.5140	
d	$\left(4d_{3/2}^{-1}\,5p_{1/2}\right)_{J=1}$	$E1$		12.73	12.6908	12.6932	12.7772	
e	$\left(4d_{3/2}^{-1}\,5p_{3/2}\right)_{J=1}$	$E1$	12.20	12.22	12.2103	12.2177	12.2250	
f	$\left(4d_{5/2}^{-1}\,4f_{5/2}\right)_{J=1}$	$E1$	13.03	13.07	13.0232†	13.2000	13.2007	
g	$\left(4d_{3/2}^{-1}\,4f_{5/2}\right)_{J=1}$	$E1$	12.39	12.38	12.4001	12.4439	12.4983	
h	$\left(4d_{5/2}^{-1}\,4f_{7/2}\right)_{J=1}$	$E1$	10.14*	9.77	10.1391	9.8299	10.2309	

were obtained with electron energies of 110 and 150 eV for palladium-like I^{7+} and Ba^{10+}, respectively, which are above the threshold energies to generate the palladium-like ions (88 eV for I and 147 eV for Ba [50]). For I^{7+}, two experimental spectra (13–20 and 23–29 nm) were measured individually by moving the CCD position as the transitions spread beyond the wavelength range covered by a fixed CCD position. In the experimental barium spectrum, we simultaneously observed the reference Kr^{8+} lines [51] from the residual krypton gas. The simulation spectra were calculated for electron energies of 110 and 150 eV for I^{7+} and Ba^{10+}, respectively, and an electron density of 10^{10} cm^{-3}, which is a typical density in CoBIT. Each line width was convolved with a full width at half maximum (FWHM) of 0.2 eV, corresponding to 0.01 nm at 25 nm. Although the absolute wavelength for each line differs slightly between the experiment and the simulation, the experimental spectral features are well reproduced by the simulation spectra. From the comparison, we assigned the observed lines as shown by the labels a–h used in Fig. 2. In Fig. 3(a), the emission lines arising from the same transition are connected by the dashed lines between I^{7+} and Ba^{10+}. The color for each dashed line corresponds to the color code of the excited state shown in Fig. 2. The emission lines in Ba^{10+} are shifted to the shorter wavelength side with respect to the corresponding I^{7+} as expected from the general Z dependence. Additionally, it is clearly shown that the shifts greatly depend on the electron configuration in the excited state. In particular, the $4d^{-1}4f$ states have a smaller energy

shift than the $4d^{-1}5s$ and $4d^{-1}5p$ states due to the difference in the principal quantum number. As a result, the transitions from $4d^{-1}4f$ and $4d^{-1}5p$ to the ground state in Ba^{10+} are overlapped.

In Table I, the wavelengths of the observed lines are listed with previous experimental values [41,52–54]. The upper level of each transition is given in the jj-coupling scheme based on the present calculated results obtained with FAC. We have also compared our present results with previous theoretical calculations [42,43]. For I^{7+}, Ivanova [42] calculated the energy levels using relativistic perturbation theory (RPTMP) with a model potential. For Ba^{10+}, Safronova *et al.* [43] performed a detailed systematic study of transition energies and transition probabilities using the first- and second-order relativistic many-body perturbation theory (RMBPT). It is noted that in this paper the transition wavelength values are listed in descending order regardless of the assignment given in the previous paper [41]. In the present FAC structure calculations, we have included only the important configurations; however, comparison with experimental and previous theoretical results shows that the accuracy is good enough to reproduce spectral features. The previous experiments were performed with a vacuum spark plasma or a laser-produced plasma, where only the prominent $E1$ transitions could be observed. The present experiment provides the first direct observation of the electric-quadrupole ($E2$) transitions from $4d^{-1}5s$. The previous wavelength values listed in the table for
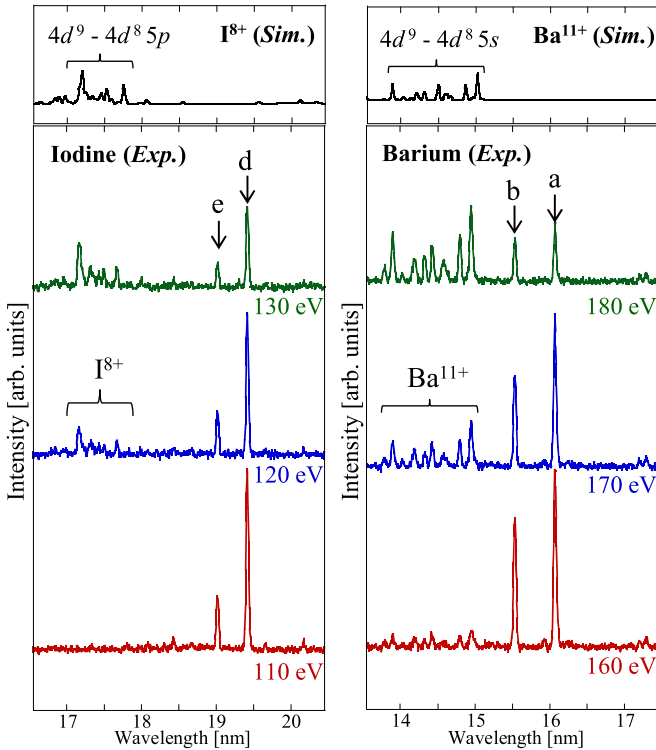
FIG. 4. Electron beam dependence of EUV emission spectra with spectral simulations for I^{8+} and Ba^{11+}. The annotations a, b, d, and e represent the palladium-like ion transitions which were labeled in Figs. 1 and 2.

FIG. 5. Electron beam dependence of visible emission spectra of I^{8+} and Ba^{11+} after background subtraction. In the iodine spectra, the hydrogen Balmer α transition (656 nm) derived from the dissociative fragment of CH_3I was observed.

the $4d^{10}$-$4d^{-1}5s$ transitions are derived from the $4d^{-1}5s$ level energy indirectly determined by using the Ritz combination principle. As shown in Table I, the present experimental wavelengths agree with previous measurements, including five transitions for which the Ritz wavelength is given for the previous value.

Figure 4 shows the EUV spectra at several electron beam energies along with CR model simulation spectra of rhodium-like I^{8+} and Ba^{11+} which were generated by removing one electron from the palladium-like ions. The simulation spectra were calculated for electron energies of 150 and 180 eV for I^{8+} and Ba^{11+}, respectively, and an electron beam density of 10^{10} cm^{-3} was assumed. By comparing the experimental and simulation spectra, we assign the $4d^9$-$4d^85p$ lines of I^{8+} and the $4d^9$-$4d^85s$ lines of Ba^{11+}. According to the FAC calculation and the NIST database [50], ionization energies from the ground state of palladium-like I^{7+} and Ba^{10+} are 151 and 241 eV, respectively. However, the presence of both I^{8+} and Ba^{11+} were confirmed at energies lower than the ionization energy from the ground state of the palladium-like ions. Although the result indicates the existence of an ionization process from metastable states of palladium-like ions, the linearity between the number of generated rhodium-like ions and emission intensity of EUV transitions with an electron jumping is not generally ensured because such transitions often show a strong dependence on the electron beam energy without ionization processes [47,48,55]. Thus for a more detailed consideration, we observed the visible $M1$ transitions of I^{8+} and Ba^{11+}.
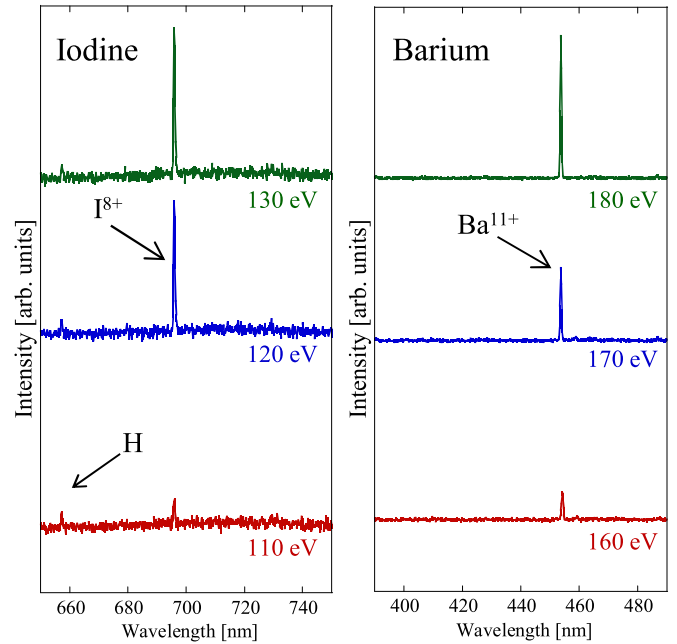
Figure 5 shows the visible emission spectra of I^{8+} and Ba^{11+} at several different electron beam energies. The Ba^{11+} line at 454 nm is the magnetic-dipole ($M1$) transition between fine-structure levels ($J = 5/2$–$3/2$) in the ground term (^2D), which was observed and identified in our previous study [32]. In the present iodine spectra, a prominent line was observed at around 695 nm. By comparison with a theoretical value obtained with relativistic many-body perturbation theory (RMBPT), we assigned this line to the $M1$ transition ($4d^{-1}$: $^2D_{5/2}$ - $^2D_{3/2}$) in I^{8+} similarly to the Ba^{11+} line. Table II lists a summary of the present and previous studies for the energy between the fine-structure levels. The previous theoretical value by Joshi *et al.* [56] was obtained by the relativistic Hartree-Fock equation. The present theoretical value was calculated with RMBPT based on FAC [5,57]. In the present RMBPT calculation, the perturbation expansion, up to second order, includes the configurations from the single and double excitation from $4d^9$ and $4d^8$ $4f$, $4d^8$ $5l$ ($l = s, p, d$). For the single and double excitation, the maximum principle quantum number was set to 30 and 20, respectively. The maximum orbital quantum number was set to 15. We

TABLE II. Fine-structure splitting (cm^{-1}) of $4d^{-1}$ $^2D_{5/2}$ - $^2D_{3/2}$ in rhodium-like I^{8+}. The uncertainties in the previous indirect experiments are not given. The uncertainty of the present experimental value is estimated to be 1 cm^{-1}.

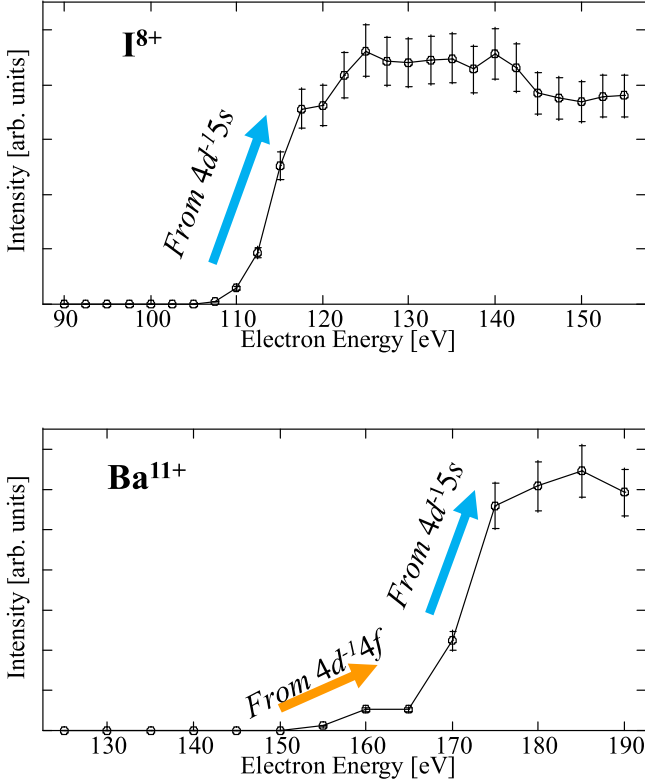|	Theory	Expt. (direct)	Expt. (indirect)
Even-Zohar [52]			14403
Joshi [56]	14362		14362
This work	14388	14392.5	

FIG. 6. Electron beam energy dependence of the intensities of the visible lines ($4d^{-1} : {}^2D_{5/2}$ - ${}^2D_{3/2}$) in I^{8+} and Ba^{11+}. Each data set is normalized to the electron density.

followed the procedure discussed by Fei *et al.* [58], and systematically increased the expansion space step by step to get the convergence and accuracy of our calculations. The previous experiments [52,56] were performed by observation of extreme ultraviolet emission lines and analyses of the resulting spectra. The present experimental value was determined by an accurate measurement technique with simultaneously observed reference lines of neutral Ne atoms [59]. The uncertainty, including the systematic error, was estimated to be 1 cm^{-1}. Although the present experimental value differs from the previous experimental values, it is difficult to discuss the significance at present because uncertainties for the previous values were not given. However, it should be noted that

both previous experimental values were indirectly determined, whereas our experiment is the first direct determination of the energy level. Thus we consider that the value should be revised to 14392.5 (1.0) cm^{-1}.

Figure 6 shows the electron beam energy dependence of the visible line intensities for rhodium-like I^{8+} and Ba^{11+}. In these measurements, the electron current was kept constant (2 mA for I and 3 mA for Ba), and the intensity is normalized to the relative electron density assuming that the electron beam radius is independent of the energy. The error bars in the figure were estimated from the uncertainty in the beam current measured with an analog meter. According to the CR model calculation, the intensity of the $M1$ transition in rhodium-like ions does not have a strong dependence on electron beam energy for the energy range studied. Thus, it can be considered that the intensity mainly depends on the number of rhodium-like ions trapped in CoBIT. The result indicates the existence of an ionization process from metastable states of palladium-like ions. Moreover, the intensity of Ba^{11+} shows a two-stage increment. To understand the ionization process, we summarized our theoretically calculated results for the population of the ground and metastable states of palladium-like I^{7+} and Ba^{10+} in Table III. As seen in the table, the theoretical population of the $4d^{-1}5s$ levels is large for both I^{7+} and Ba^{10+}. Therefore, the ionization from $4d^{-1}5s$ should be possible also at an electron energy below the ionization threshold from the $4d^{10}$ ground state. In Ba^{10+}, the C, D and E levels in $4d^{-1}4f$ also have a significant population; thus the ionization should be possible at even lower energies. The first stage of the two-stage increment is thus considered to have been realized by ionization from $4d^{-1}4f$, whereas the second stage is from $4d^{-1}5s$. On the other hand, for I^{7+}, the population of the C–E levels is so small that ionization from $4d^{-1}4f$ is practically impossible. We note that the width and the shift (<10 eV) of the electron beam energy are small enough as to not affect the above discussion.

To study the experimentally observed difference of the ionization processes between iodine and barium ions in Co-BIT, Fig. 7(a) shows calculated lifetimes of the longest-lived levels $A : (4d^{-1}5s)_{J=3}$ and $C : (4d^{-1}4f)_{J=6}$ as a function of the atomic number Z. The lifetime of the $(4d^{-1}5s)_{J=3}$ level monotonically and gradually decreases as Z increases due to the increase in the transition energy for the main decay path to the $4d^{10}$ ground state. On the other hand, the

TABLE III. Summary of calculation results for the metastable states with FAC. The lifetimes τ are given by summing the inverse of the decay rates for every de-excitation channels. ρ is the population in the plasma. The population values lower than 0.1 % are not shown. In the CR model calculation, an electron density of 10^{10} cm^{-3} and electron beam energies of 110 eV for I^{7+} and 150 eV for Ba^{10+} were assumed. I_{ene} is the binding energy. The labels A–E are defined in Fig. 1. The label G means the ground state.

Label	Level	I ($Z = 53$)			Ba ($Z = 56$)		
		τ (s)	ρ (%)	I_{ene} (eV)	τ (s)	ρ (%)	I_{ene} (eV)
A	$\left(4d_{5/2}^{-1} 5s_{1/2}\right)_{J=3}$	$3.6 \times 10^{+3}$	17.64	103	$2.3 \times 10^{+2}$	12.91	165
B	$\left(4d_{3/2}^{-1} 5s_{1/2}\right)_{J=1}$	3.3×10^{-2}	1.92	102	8.1×10^{-3}	0.81	162
C	$\left(4d_{5/2}^{-1} 4f_{7/2}\right)_{J=6}$	3.2×10^{-4}	0.13	73	$1.6 \times 10^{+2}$	6.51	144
D	$\left(4d_{5/2}^{-1} 4f_{5/2}\right)_{J=5}$	1.9×10^{-4}		73	6.8×10^{-1}	2.74	144
E	$\left(4d_{5/2}^{-1} 4f_{7/2}\right)_{J=5}$	2.3×10^{-4}		71	2.7×10^{-2}	1.10	141
G	$(4d^{10})_{J=0}$		80.11	150		75.48	241

(a) *Z* dependence of the lifetimes
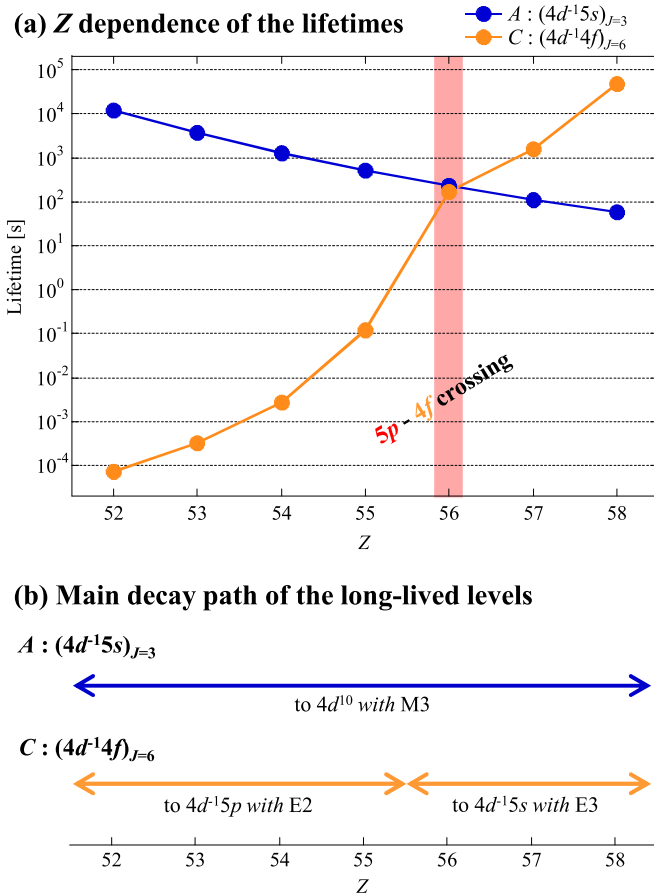

(b) Main decay path of the long-lived levels

FIG. 7. (a) Atomic number dependence of the lifetimes of the long-lived levels $A : (4d^{-1}5s)_{J=3}$ and $C : (4d^{-1}4f)_{J=6}$ for $Z = 52$–58. The Z number (Ba: $Z = 56$) shaded red has a level crossing of $4d^{-1}5p$-$4d^{-1}4f$. (b) Main decay path for each long-lived level.

lifetime of the $(4d^{-1}4f)_{J=6}$ level increases with Z due to the decrease in the transition energy for the main decay path to the $4d^{-1}5l$ ($l = s, p$) levels. In addition, due to the $5p$-$4f$ crossing at $Z = 56$, the main decay path of the $(4d^{-1}4f)_{J=6}$ level changes from $E2$ decay to $(4d^{-1}5p)_{J=4}$ for $Z < 56$ to $E3$ decay to $(4d^{-1}5s)_{J=3}$ for $Z \geqslant 56$. The significant difference in the decay lifetime between $E2$ and $E3$ causes the sharp increase of the lifetime between $Z = 55$ and 56. As a result, for Ba ($Z = 56$), the lifetime of both the $(4d^{-1}5s)_{J=3}$ and $(4d^{-1}4f)_{J=6}$ levels is long enough to reveal significant populations which are responsible for the observed multistep ionization process. On the other hand, for I ($Z = 53$), $E2$ decay to $(4d^{-1}5p)_{J=4}$ quenches the population of the $(4d^{-1}4f)_{J=6}$ level, which results in only single-step ionization from the $(4d^{-1}5s)_{J=3}$ level.

V. SUMMARY AND OUTLOOK

In summary, we investigated the level structures of palladium-like I^{7+} and Ba^{10+} with a compact EBIT. In the extreme ultraviolet spectra, we detected several prominent lines including those that, to our knowledge, had never been directly observed before. In order to assign the observed lines,

we performed a spectral simulation based on CR modeling and clearly characterized the complicated spectra having a $5p$-$4f$ level crossing. The experimental wavelengths of the assigned prominent lines from $4d^{-1}5s$, $4d^{-1}5p$, and $4d^{-1}4f$ configurations to the $4d^{10}$ ground state show good agreement with previously reported values [41,52–54]. The extreme ultraviolet spectra and its analyses clearly provide the energy structure of $4d^{-1}5s$, $4d^{-1}5p$, and $4d^{-1}4f$ configurations and evidence for the $5p$-$4f$ level crossing at $Z = 56$ (Ba^{10+}). Additionally, we observed the electron beam energy dependence of the prominent visible line ($4d^{-1} : {}^2D_{5/2}$-${}^2D_{3/2}$) of rhodium-like I^{8+} and Ba^{11+}. The energy dependence of the line intensities indicated the existence of indirect ionization processes via the metastable states in palladium-like I^{7+} and Ba^{10+}. We identified the electron configurations of the metastable states involved in the ionization processes by comparison with theoretically calculated populations in the EBIT plasma. In I^{7+}, only the $4d^{-1}5s$ configuration contributed to the indirect ionization process, whereas the ionization of Ba^{10+} occurred from the metastable states not only in $4d^{-1}5s$ but also $4d^{-1}4f$. We emphasize that it has been experimentally demonstrated that the $5p$-$4f$ level crossing causes a significant atomic number dependence of the lifetime of the metastable states, and the result provides a new aspect of $5l$-$4f$ level crossings.

The present investigation adds to the experimental evidence on the important role of metastable states in the population dynamics of plasmas, and shows one clear example of their effects in spectroscopic plasma diagnostics. In addition, such long-lived levels can be applied to laser spectroscopy; as an example, a method using nickel-like ions having a $3d^{10}$ closed shell ground state has been proposed [60]. This proposal extended the spectroscopic method, which was demonstrated by using the $2s$ level of hydrogen-like N^{6+} [61], to long-lived metastable levels. Furthermore, we consider that the long lifetimes allow for applying to the laser spectroscopy of ions trapped in not only an EBIT but also a Penning trap [62,63] and a Coulomb crystal [64–68], and it is possible to measure various transitions between excited levels with high precision. In particular, I^{7+} is a practical target for the laser spectroscopy because it has a highly populated metastable state $(4d_{5/2}^{-1}\,5s_{1/2})_{J=3}$ and a pumping transition $[(4d_{5/2}^{-1}\,5s_{1/2})_{J=3} \rightarrow (4d_{3/2}^{-1}\,5s_{1/2})_{J=2} : \lambda = 567$ nm$]$ for which a wavelength-tunable laser is easily available. The development of this spectroscopic method and the results will contribute to a systematic study for an improved understanding of relativistic many-electron atomic theory.

[1] T. Watanabe, J. Phys. B: Conf. Ser. **163**, 012002 (2009).

[2] Y. Ralchenko, Plasma Fusion Res. **8**, 2503024 (2013).

[3] P. Beiersdorfer, J. Phys. B: At. Mol. Opt. Phys. **48**, 144017 (2015).

[4] W. Biel, R. Albanese, R. Ambrosino, M. Ariola, M. V. Berkel, I. Bolshakova, K. J. Brunner, R. Cavazzana, M. Cecconello, S. Conroy, A. Dinklage, I. Duran, R. Dux, T. Eade, S. Entler, G. Ericsson, E. Fable, D. Farina, L. Figini, C. Finotti *et al.*, Fusion Eng. Des. **146**, 465 (2019).

[5] M. F. Gu, Can. J. Phys. **86**, 675 (2008).

[6] J. C. Berengut, V. A. Dzuba, and V. V. Flambaum, Phys. Rev. Lett. **105**, 120801 (2010).

[7] M. G. Kozlov, M. S. Safronova, J. R. Crespo López-Urrutia, and P. O. Schmidt, Rev. Mod. Phys. **90**, 045005 (2018).

[8] J. C. Berengut, V. A. Dzuba, V. V. Flambaum, and A. Ong, Phys. Rev. Lett. **106**, 210802 (2011).

[9] J. C. Berengut, V. A. Dzuba, V. V. Flambaum, and A. Ong, Phys. Rev. A **86**, 022517 (2012).

[10] V. A. Dzuba, A. Derevianko, and V. V. Flambaum, Phys. Rev. A **86**, 054502 (2012).

[11] M. S. Safronova, V. A. Dzuba, V. V. Flambaum, U. I. Safronova, S. G. Porsev, and M. G. Kozlov, Phys. Rev. Lett. **113**, 030801 (2014).

[12] M. S. Safronova, V. A. Dzuba, V. V. Flambaum, U. I. Safronova, S. G. Porsev, and M. G. Kozlov, Phys. Rev. A **90**, 042513 (2014).

[13] M. S. Safronova, V. A. Dzuba, V. V. Flambaum, U. I. Safronova, S. G. Porsev, and M. G. Kozlov, Phys. Rev. A **90**, 052509 (2014).

[14] V. A. Dzuba, V. V. Flambaum, and H. Katori, Phys. Rev. A **91**, 022119 (2015).

[15] U. I. Safronova, V. V. Flambaum, and M. S. Safronova, Phys. Rev. A **92**, 022501 (2015).

[16] V. A. Dzuba and V. V. Flambaum, Phys. Rev. A **93**, 052517 (2016).

[17] D. K. Nandy and B. K. Sahoo, Phys. Rev. A **94**, 032504 (2016).

[18] C. Cheung, M. S. Safronova, S. G. Porsev, M. G. Kozlov, I. I. Tupitsyn, and A. I. Bondarev, Phys. Rev. Lett. **124**, 163001 (2020).

[19] A. Windberger, J. R. Crespo Lopez-Urrutia, H. Bekker, N. S. Oreshkina, J. C. Berengut, V. Bock, A. Borschevsky, V. A. Dzuba, E. Eliav, Z. Harman, U. Kaldor, S. Kaul, U. I. Safronova, V. V. Flambaum, C. H. Keitel, P. O. Schmidt, J. Ullrich, and O. O. Versolato, Phys. Rev. Lett. **114**, 150801 (2015).

[20] H. Bekker, O. O. Versolato, A. Windberger, N. S. Oreshkina, R. Schupp, T. M. Baumann, Z. Harman, C. H. Keitel, P. O. Schmidt, and J. Ullrich, J. Phys. B: At. Mol. Opt. Phys. **48**, 144018 (2015).

[21] T. Nakajima, K. Okada, M. Wada, V. A. Dzuba, M. S. Safronova, U. I. Safronova, N. Ohmae, H. Katori, and N. Nakamura, Nucl. Instrum. Methods B **408**, 118 (2017).

[22] H. Bekker, A. Borschevsky, Z. Harman, C. H. Keitel, T. Pfeifer, P. O. Schmidt, J. R. Crespo López-Urrutia, and J. C. Berengut, Nat. Commun. **10**, 5651 (2019).

[23] R. E. Marrs, M. A. Levine, D. A. Knapp, and J. R. Henderson, Phys. Rev. Lett. **60**, 1715 (1988).

[24] A. Butler, A. J. Gonsalves, C. M. McKenna, D. J. Spence, S. M. Hooker, S. Sebban, T. Mocek, I. Bettaibi, and B. Cros, Phys. Rev. A **70**, 023821 (2004).

[25] E. P. Ivanova, Phys. Rev. A **82**, 043824 (2010).

[26] R. X. Schüssler, H. Bekker, M. Braß, H. Cakir, J. R. Crespo López-Urrutia, M. Door, P. Filianin, Z. Harman, M. W. Haverkort, W. J. Huang, P. Indelicato, C. H. Keitel, C. M. König, K. Kromer, M. Müller, Y. N. Novikov, A. Rischka, C. Schweiger, S. Sturm, S. Ulmer, S. Eliseev, and K. Blaum, Nature (London) **581**, 42 (2020).

[27] Y. Kobayashi, D. Kato, H. A. Sakaue, I. Murakami, and N. Nakamura, Phys. Rev. A **89**, 010501(R) (2014).

[28] Y. Kobayashi, K. Kubota, K. Omote, A. Komatsu, J. Sakoda, M. Minoshima, D. Kato, J. Li, H. A. Sakaue, I. Murakami, and N. Nakamura, Phys. Rev. A **92**, 022510 (2015).

[29] D. Kato, H. A. Sakaue, I. Murakami, and N. Nakamura, Nucl. Instrum. Methods B **408**, 16 (2017).

[30] M. Mita, H. A. Sakaue, D. Kato, I. Murakami, and N. Nakamura, J. Phys.: Conf. Ser. **875**, 012019 (2017).

[31] Q. Lu, J. He, H. Tian, M. Li, Y. Yang, K. Yao, C. Chen, J. Xiao, J. G. Li, B. Tu, and Y. Zou, Phys. Rev. A **99**, 042510 (2019).

[32] J. Sakoda, A. Komatsu, H. Kikuchi, and N. Nakamura, Phys. Scr. **2011**, 014011 (2011).

[33] A. Windberger, F. Torretti, A. Borschevsky, A. Ryabtsev, S. Dobrodey, H. Bekker, E. Eliav, U. Kaldor, W. Ubachs, R. Hoekstra, J. R. Crespo López-Urrutia, and O. O. Versolato, Phys. Rev. A **94**, 012506 (2016).

[34] F. Torretti, A. Windberger, A. Ryabtsev, S. Dobrodey, H. Bekker, W. Ubachs, R. Hoekstra, E. V. Kahl, J. C. Berengut, J. R. C. López-Urrutia, and O. O. Versolato, Phys. Rev. A **95**, 042503 (2017).

[35] A. Borovik, Jr., A. Müller, S. Schippers, I. Bray, and D. V. Fursa, J. Phys. B: At. Mol. Opt. Phys. **42**, 025203 (2009).

[36] J. Rausch, A. Becker, K. Spruck, J. Hellhund, A. Borovik, Jr., K. Huber, S. Schippers, and A. Müller, J. Phys. B: At. Mol. Opt. Phys. **44**, 165202 (2011).

[37] A. Borovik, Jr., B. Ebinger, D. Schury, S. Schippers, and A. Müller, Phys. Rev. A **93**, 012708 (2016).

[38] V. Jonauskas, A. Kynienė, S. Kučas, S. Pakalka, Š. Masys, A. Prancikevičius, A. Borovik, Jr., M. F. Gharaibeh, S. Schippers, and A. Müller, Phys. Rev. A **100**, 062701 (2019).

[39] H. A. Sakaue, D. Kato, I. Murakami, H. Ohashi, and N. Nakamura, Phys. Rev. A **100**, 052515 (2019).

[40] J. Sugar and V. Kaufman, Phys. Scr. **26**, 419 (1982).

[41] S. S. Churilov, A. N. Ryabtsev, W.-Ü. L. Tchang-Brillet, and J.-F. Wyart, Phys. Scr. **66**, 293 (2002).

[42] E. P. Ivanova, At. Data Nucl. Data Tables **95**, 786 (2009).

[43] U. I. Safronova, R. Bista, R. Bruch, and H. Merabet, Can. J. Phys. **86**, 131 (2008).

[44] N. Nakamura, H. Kikuchi, H. A. Sakaue, and T. Watanabe, Rev. Sci. Instrum. **79**, 063104 (2008).

[45] C. Yamada, K. Nagata, N. Nakamura, S. Ohtani, S. Takahashi, T. Tobiyama, M. Tona, M. Sakurai, A. P. Kavanagh, and F. J. Currell, Rev. Sci. Instrum. **77**, 066110 (2006).

[46] G. Y. Liang, T. M. Baumann, J. R. Crespo López-Urrutia, S. W. Epp, H. Tawara, A. Gonchar, P. H. Mokler, G. Zhao, and J. Ullrich, Astrophys. J. **696**, 2275 (2009).

[47] T. Tsuda, E. Shimizu, S. Ali, H. A. Sakaue, D. Kato, I. Murakami, H. Hara, T. Watanabe, and N. Nakamura, Astrophys. J. **851**, 82 (2017).

[48] M. Monobe, H. A. Sakaue, D. Kato, I. Murakami, H. Hara, T. Watanabe, and N. Nakamura, X-ray Spectrom. **49**, 511 (2020).

[49] H. Ohashi, J. Yatsurugi, H. A. Sakaue, and N. Nakamura, Rev. Sci. Instrum. **82**, 083103 (2011).

[50] A. Kramida, Y. Ralchenko, J. Reader, and NIST ASD Team, NIST atomic spectra database (version 5.7), http://physics.nist.gov/asd (2019).

[51] J. Reader, N. Acquista, and V. Kaufman, J. Opt. Soc. Am. B **8**, 538 (1991).

[52] M. Even-Zohar and B. S. Fraenkel, J. Phys. B: At. Mol. Phys. **5**, 1596 (1972).

[53] Y. N. Joshi, Th. A. M. van Kleef, and C. G. Mahajan, J. Opt. Soc. Am. B **4**, 1306 (1987).

[54] S. S. Churilov, V. I. Azarov, A. N. Ryabtsev, W-Ü. L. Tchang-Brillet, and J.-F. Wyart, Phys. Scr. **61**, 420 (2000).

[55] E. Shimizu, S. Ali, T. Tsuda, H. A. Sakaue, D. Kato, I. Murakami, H. Hara, T. Watanabe, and N. Nakamura, Astron. Astrophys. **601**, A111 (2017).

[56] Y. N. Joshi and Th. A. M. van Kleef, J. Opt. Soc. Am. **70**, 1344 (1980).

[57] M. F. Gu, Astrophys. J. Suppl. Ser. **169**, 154 (2007).

[58] Z. Fei, W. Li, J. Grumer, Z. Shi, R. Zhao, T. Brage, S. Huldt, K. Yao, R. Hutton, and Y. Zou, Phys. Rev. A **90**, 052517 (2014).

[59] N. Kimura, R. Kodama, K. Suzuki, S. Oishi, M. Wada, K. Okada, N. Ohmae, H. Katori, and N. Nakamura, Phys. Rev. A **100**, 052508 (2019).

[60] Y. Ralchenko, Nucl. Instrum. Methods B **408**, 38 (2017).

[61] K. Hosaka, D. N. Crosby, K. Gaarde-Widdowson, C. J. Smith, J. D. Silver, T. Kinugawa, S. Ohtani, and E. G. Myers, Phys. Rev. A **69**, 011802(R) (2004).

[62] V. Mäckel, R. Klawitter, G. Brenner, J. R. Crespo López-Urrutia, and J. Ullrich, Phys. Rev. Lett. **107**, 143002 (2011).

[63] K. Schnorr, V. Mäckel, N. S. Oreshkina, S. Augustin, F. Brunner, Z. Harman, C. H. Keitel, J. Ullrich, and J. R. Crespo López-Urrutia, Astrophys. J. **776**, 121 (2013).

[64] L. Gruber, J. P. Holder, J. Steiger, B. R. Beck, H. E. DeWitt, J. Glassman, J. W. McDonald, D. A. Church, and D. Schneider, Phys. Rev. Lett. **86**, 636 (2001).

[65] Z. Andelkovic, R. Cazan, W. Nörtershäuser, S. Bharadia, D. M. Segal, R. C. Thompson, R. Jöhren, J. Vollbrecht, V. Hannen, and M. Vogel, Phys. Rev. A **87**, 033423 (2013).

[66] L. Schmöger, O. O. Versolato, M. Schwarz, M. Kohnen, A. Windberger, B. Piest, S. Feuchtenbeiner, J. Pedregosa-Gutierrez, T. Leopold, P. Micke, A. K. Hansen, T. M. Baumann, M. Drewsen, J. Ullrich, P. O. Schmidt, and J. R. Crespo López-Urrutia, Science **347**, 1233 (2015).

[67] L. Schmöger, M. Schwarz, T. M. Baumann, O. O. Versolato, B. Piest, T. Pfeifer, J. Ullrich, P. O. Schmidt, and J. R. Crespo López-Urrutia, Rev. Sci. Instrum. **86**, 103111 (2015).

[68] P. Micke, T. Leopold, S. A. King, E. Benkler, L. J. Spieß, L. Schmöger, M. Schwarz, J. R. Crespo López-Urrutia, and P. O. Schmidt, Nature (London) **578**, 60 (2020).